Mobilya ve Ahşap Malzeme Araştırmaları Dergisi
Furniture and Wooden Material Research Journal
Research Article - Araştırma Makalesi 2025 - 8(1), 143-155

Performance and deformation behavior of a master jig on circular saw machine using finite element method

Asibong Asibong Icha[1*], Simon Ogbeche Odey[1]

ABSTRACT: This study investigates the performance, stress distribution, deformation and potential failure modes of a newly developed Master Jig (MJ) designed for circular saw machine operations. The MJ comprises three components: the master jig body (MJB), the master jig accessories (MJA) and the master jig guide (MJG). The jig was modelled and simulated under applied static loads of 520 N and 600 N using SOLIDWORKS software. The MJ performance was evaluated, results were recorded, and a deformation graph was presented and shape displayed in true and defined scales of 0.135238 and 0.036047, respectively. The analysis shows that, maximum directional deformations at 520 N and 600 N were 8.463×10^{2} mm and 3.197×10^{3} mm respectively, elastic strains at 6.540 x 10 and 1.433 x 10, von mises stresses at 2.580×10^{6} MPa and 3.930×10^{7} MPa respectively, the Yield Strengths at 2.000×10^{7} MPa and 3.930×10^{7} MPa respectively, and the factor of safety at 31 and 11 respectively. The study underscores the potential of finite element modelling in the predictive design of woodworking jigs.

Keywords: Master Jig, Finite Element Modelling, Circular Saw Machine

Sonlu eleman yöntemleri kullanılarak dairesel testere makinesinde bir ana şablonun performans ve deformasyon davranışı

ÖZ: Bu çalışmada, dairesel testere tezgahı operasyonları için tasarlanmış yeni geliştirilmiş bir Ana Jig'in (MJ) performansı, gerilim dağılımı, deformasyonu ve potansiyel arıza modları araştırılmıştır. Geliştirilen MJ üç bileşenden oluşmaktadır: Ana Kalıp Gövdesi (MJB), Ana Kalıp Aksesuarları (MJA) ve Ana Kalıp Kılavuzu (MJG). MJ'nin modellenmesi, simülasyonu ve analizi için SOLIDWORKS yazılımı kullanılmış ve sırasıyla 520N ve 600N statik yükler uygulanmıştır. MJ'nin performansı değerlendirilmiş, sonuçlar kaydedilmiş, deformasyon grafiği sunulmuş ve şekli gerçek ve belirlenmiş ölçeklerde gösterilmiştir. Analizler, maksimum yönlendirilmiş deformasyonların sırasıyla 8.463×10^{2} mm ve 3.197×10^{3} mm, eşdeğer elastik şekil değişimlerinin 6.540×10^{0} ve 1.433×10^{1}, von Mises gerilmelerinin 2.580×10^{6} MPa ve 3.930×10^{7} MPa, akma dayanımlarının 2.000×10^{7} N/m² ve 3.930×10^{7} N/m², güvenlik katsayısının ise sırasıyla 31 ve 11 olduğunu göstermektedir. Çalışma, ağaç işleme fikstürlerinin tahmini tasarımında sonlu elemanlar modellemesinin potansiyelini vurgulamaktadır.

Anahtar kelimeler: Ana Kalıp, Sonlu Eleman Metodu, Daire Testere Makinesi

Article history: Received: 23.03.2025, Revised:21.06.2025, Accepted: 22.06.2025, Published: 27.06.2025, *ichaasibonga@gmail.com
[1]University of Cross River State, Department of Wood Products Engineering, Calabar/ Nigeria

To cite: Icha, A.A., and Odey S.O., (2025). Performance and deformation behavior of a master jig on circular saw machine using finite element method, *Furniture and Wooden Material Research Journal*, 8 (1), 143-155, DOI: 10.33725/mamad.1663809

1. Introduction

The intricacies of predicting the performance and potential deformational behavior of wood and wood-based products have posed challenges that have, until now, relied heavily on intuition and experience (DeCristoforo, 1988; Okpala and Okechukwu, 2015; Massaro et al., 2023; Icha et al., 2024). Massive efforts have been made for several years to close the knowledge gap and enhance the techniques required to make wood more predictable (Falk and Itani, 1989; Brischke, 2021; Fiedler et al., 2023). Appraisal of the capacity of carpentry joints using Finite Element (FE) models had been investigated, compared to experimental results with acceptable prediction capacity (Massaro et al., 2022). Huber et al (2023) presented a technique based on X-ray computed tomography scans for recreating the structural features in wood boards. They suggest that eventually, using the technique for sawing logs could aid analyses of boards. Nailed connection in wood (Hong and Barrett, 2010), screws (Hu et al., 2022) crack propagation (Qiu et al., 2013), water absorption (Salin, 2008), wood fracture mechanics (Vasic, 2005), and many other behaviors have been presented (Blomqvist et al., 2023). Autengruber et al. (2021) developed a finite-element-based simulation approach to better understand the failure mechanics of wood-based composite and to support a targeted optimization of new cross-section types of I-joist beams. The performance of the modelling approach was reported as giving a very good prediction of stiffness values.

Frontini (2023) presented finite element models of wooden roofs with two main scenarios in an attempt to characterize the behavior of wooden connections in the diaphragm. The first scenario considered only the frame with line loads, while the second scenario considered that the wooden boards incorporating planks affected the performance of the structure. The result of their work agrees with the use of FEM to analyse, model and simulate the behaviors of wooden members. Blomqvist et al., (2023) created the FE model to study the bending process of a laminated veneer product. The veneers, which were modelled after the experimental ones with laminates of different thicknesses made of peeled veneers of European beech, had corresponding results. Zhong et al., (2021) simulated the deformation behavior of wood under axial and transverse compression conditions with representative volume elements (RVE). The simulation was able to reflect wood compression behavior from its results. This gives credits to the versatility and reliability of FEM as a tool for analysing and simulating the complex behaviors of wooden materials and structures under various conditions, thereby advancing both theoretical understanding and practical applications in wood material utilisation.

Woodworkers and engineers alike have learned that the performance and dependability of this essential component are not to be taken for granted. However, only big manufacturing organizations in developing nations have the expertise and resources to implement these contemporary technologies (Tankut et al., 2014). Thus, the Master jig's performance, as well as its potential deformation behavior, denote critical factors that directly affect the quality and safety of woodworking undertakings (Icha and Odey, 2024a; Fleming, 2020). Our study aims to address this by utilizing simulation and predictive modelling as effective methods for understanding the Master Jig's behavior in operation on the circular saw machine (Icha and Odey, 2024a; Autengruber, et al., 2021; Hernández et al., 2014). By using this novel approach, we hope to predict the jig's performance as well as solve the mystery of possible failure behaviors that have long evaded conventional techniques (Yıldırım et al., 2016; Autengruber, et al., 2021; Odey and Icha, 2022). Tradition and technology, craftsmanship and arithmetic, come together in this research. It is an investigation into how simulation and predictive modelling might improve our comprehension of the behavior of the Master Jig under various loads and situations. (Vasic et al., 2005; Tankut et al., 2014; Kumar et al., 2019).

Predicting the mechanical performance and deformation behavior of wood-based jigs remains a challenge, especially in environments where fabrication relies heavily on empirical methods (DeCristoforo, 1988; Icha et al., 2024). While materials such as solid wood and engineered boards have been widely used in jig fabrication, their layered anisotropic nature complicates accurate stress prediction without simulation tools. Prior studies using FEM have demonstrated promising results in understanding the behavior of woodworking component (Autengruber et al., 2021; Blomqvist et al., 2023). The master jig introduced in this study is designed to enhance both safety and precision during crosscutting and mitering operations amongst others on circular saw machines. Unlike previous jigs, this master jig integrates modular features to support local fabrication needs. This study presents the FEM- based simulation of the jig to evaluate its structural performance and identify potential deformation risk under operational loads.

2. Material and Method

2.1 Material

The materials used for this study were *Ochroma pyramidale* (Balsa) as solid wood and medium-density fiberboard (MDF) available within the environs of the research area (Calabar - Nigeria). A comprehensive detail of materials and hardware used in the construction of the master jig is detailed in Icha and Odey (2024b). Computer-aided design (CAD) was carried out using the SOLIDWORKS (2021) software interface to model the master jig. Detailed drawings are shown in Icha and Odey (2024b). The specific configurations of the master jig on the circular saw machine and direction of applied force are detailed in Fig. 1.

2.2 Finite element analysis

The SOLIDWORKS (2021) interface was used to model and simulate the MJ components. The MDF was approximated as a linear elastic isotropic material for baseline analysis. The mechanical properties of MDF, as listed in Table 1 (Hu et al., 2023), were specified for the FE model. Connection for the MJ was assigned as bolts and nuts as shown in Icha and Odey (2024b).

In this model, the base in the yz-plane is assigned a fixed geometry as an anchored point to resemble the experimental setup in Fig. 1. The jig was mounted on the circular saw table with fixed boundary conditions applied at contact points between the MJ and the saw table because the MJ's bar is slotted into the table's groove. A curvature-based mesher was employed using a minimum element size of 2 mm and 16 Jacobian points. The mesh quality, boundary conditions and loading points are shown in Fig. 3.

Loads of 520 N and 600 N were applied vertically to simulate the pressing force from a workpiece being guided by the MJ. These values were chosen based on empirical measurements of operator force during actual machine use (Fig. 1). The mesh comprised 134,792 nodes and 96,437 elements with average ratios below 1.8. This ensured high-resolution prediction of stress gradients across intricate corners and holes (Fig. 2).

Contact between jig components and the saw blade was defined using surface-to-surface contact with finite sliding and a friction coefficient of 0.33, consistent with Massaro and Malo (2020).

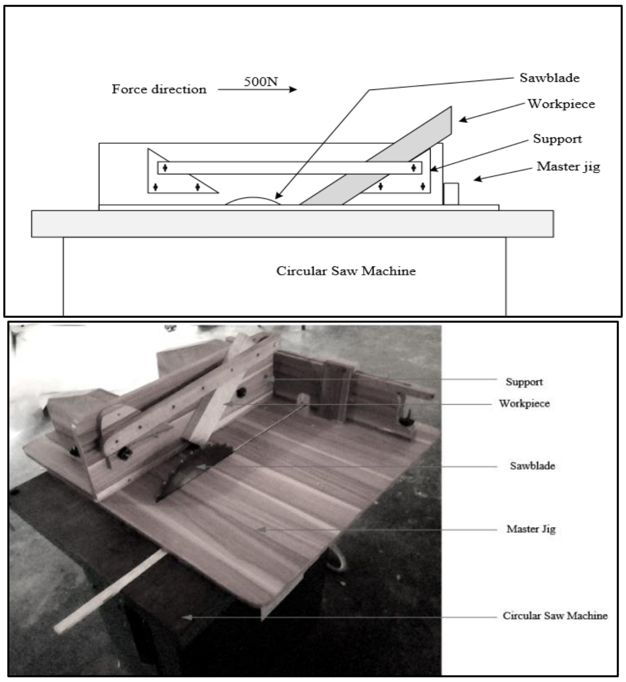

Figure 1. Experimental setup of the master jig on the circular saw machine

Table 1. Mechanical properties of MDF used in the study (Hu et al., 2023)

Property	Value	SI Units
Modulus of Elasticity	70,000	N/m^2
Poisson's Ratio	0.3	N/A
Tensile strength	0.61	N/mm^2
Yield strength	2e+07	N/m^2
Mass density	159.99	Kg/m^3
Shear modulus	3e+08	N/m^2

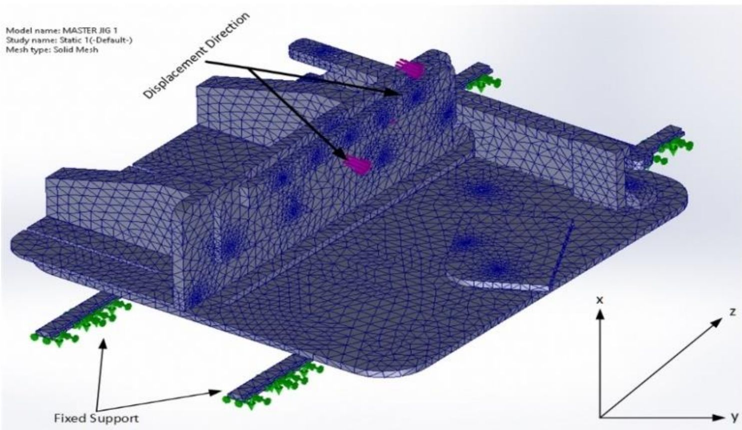

Figure 2. Mesh quality, boundary conditions and load points.

2.3 Failure criteria and equations

To evaluate the fractional behavior of the MJ under applied loads, established failure criteria were observed since materials undergo fraction when subjected to a sufficiently high load, with failure characteristics depending on the material properties and the mode of loading. In this study, varying loads of 520 and 600 N were applied on the MJ, the von Mises stress (equation 1), directional deformation (equation 2), Elastic strain (equation 3), yield stress (equation 4) and factor of safety (equation 5) were recorded (Yildirim et al., 2016). Two types of FE models were created to visualize the observed failure mode. The first represents the true scale of deformation, while the second was at a defined scale of 0.036047 and 0.135238, respectively.

Von Mises stress (σ_{vm})

$$\sigma_{vm} = \sqrt{\frac{1}{2}\,[(\sigma_x - \sigma_y)^2 + (\sigma_y - \sigma_z)^2 + (\sigma_z - \sigma_x)^2] + 6(\tau_{xy}^2 + \tau_{yz}^2 + \tau_{zx}^2)} \qquad (1)$$

Where: σ_x, σ_y, σ_z = Normal stresses in the x, y, and z directions, and τ_{xy}, τ_{yz}, τ_{zx} = Shear stresses in the respective planes

Directional deformation (Ui)

$$Ui = \frac{\sigma_i L}{E} \qquad (2)$$

Where: Ui = Deformation in direction i, σ_i = Stress in direction i, L = Initial length of the material, E = young's modulus

Elastic strain (ε_{vm})

$$\varepsilon_{vm} = \sqrt{\frac{1}{2}\,[(\varepsilon_x - \varepsilon_y)^2 + (\varepsilon_y - \varepsilon_z)^2 + (\varepsilon_z - \varepsilon_x)^2] + \frac{3}{4}(\gamma_{xy}^2 + \gamma_{yz}^2 + \gamma_{zx}^2)} \qquad (3)$$

Where: ε_x, ε_y, ε_z = Normal strains in the x, y, and z directions, and γ_{xy}, γ_{yz}, γ_{zx} = Shear strains

Yield Stress (σ_y)

$$\sigma_y = \frac{F_y}{A} \qquad (4)$$

Where: σ_y = Yield stress, F_y = Yield force, A Cross-sectional area.

Factor of safety (FoS)

$$\text{FoS} = \frac{\sigma_y}{\sigma_{max}} \qquad (5)$$

Where: σ_y = Yield stress, σ_y = Maximum applied stress

3 Results and Discussion

3.1 Simulation analysis of the master jig

Table 2 presents data from the simulation analysis carried out on the modelled master jig when loads of 520 N and 600 N are applied, respectively. The von Mises static stress, elastic strain and deformation are presented at minimum and maximum levels. The yield strength and factor of safety are also presented in the table. The von Mises stress values of the master jig indicating the internal forces acting on the MJ, resulting from the external loads of 520N and 600N, ranged from 7.833 x 10^{-4} to 5.560 x 10^{5} MPa and 1.754 x 10^{6} to 9.436 x 10^{3} MPa, respectively. The elastic strain values of the master jig, which measures the ratio of deformation to the original length of the master jig and provides an indication of its elasticity, range from 2.083 x 10^{-8} to 6.540 x 10 MPa for the 520N and 6.572 x 10^{-8} to 1.433 x 10 for 600 N. The deformation values of the master jig, which indicate the amount by which the object deforms or changes shape in a particular direction, range from 0.000 x 10 mm to 8.463 x 10^{2} mm at 520N and 0.000 x 10 mm to 3.197 x 10^{3} mm at 600N. The yield strength of the master jig, which is the maximum stress it can withstand without permanent deformation at 520, was 2.000 x 10^{7} MPa and at 600N was 3.930 x 10^{7} MPa. The factor of safety associated with the master jig at 520N and 600N is 31 and 11, respectively. These results indicate that the master jig was much stronger compared to the expected load, making it safe.

Table 2. Simulation results: maximum and minimum load values

Object Name	Load (N)	von Mises Stress (Mpa)	Elastic Strain	Deformation (mm)	Yield Stress (Mpa)	Factor of Safety
Min	520	7.833 x 10^{-4}	2.083 x 10^{-8}	0.0	2.000 x 10^{7}	31
Max		5.560 x 10^{5}	6.540 x 10	8.463 x 10^{2}		
Min	600	1.754 x 10^{6}	6.572 x 10^{-8}	0.0	3.930 x 10^{7}	11
Max		9.436 x 10^{-3}	1.433x 10	3.197x 10^{3}		

3.2 Simulation of distribution diagrams

Figs. 3 and 4 show the schematic distribution diagrams for von Mises stresses (a), elastic strain (b), and displacement (c) at 600N and 520N, respectively.

At the external load of 520N, the von Mises stresses (σ_{vm}) are observed to be higher at the stop where the force is directed and the work piece is wedged, the base slot and the lower parts of the fence. Other areas were observed to have minimal stress distribution levels. The elastic strain (ε_{vm}) distribution at the same loading condition appears to affect the same areas where the stress distributions were displaced at almost the same prominence with minimal levels of stress distribution in other areas. The displacement distribution (Ui) is observed to be highest at the point of interaction with the saw blade at over 8.463 x 10^{+2} mm varying as it moves away from the stop on both sides within the range of 5.078 x 10^{+2} mm to 8.463 x 10^{+1} mm, leaving an even distribution on other sides of the base as low as and below 1.000 x 10^{-30} mm.

At an external load of 600N, the von Mises stresses (σ_{vm}) are observed to be higher at the vertical support where the force is directed and the workpiece is wedged, the base slot and the lower parts of the fence. Other areas were observed to have minimal stress distribution levels. The elastic strain (ε_{vm}) distribution at the same loading condition appears to affect the same areas where the stress distributions were displaced, but with more prominence with minimal levels of stress distribution were observed in other areas. The displacement distribution (*Ui*) is observed to be highest at the upper part of the vertical support at over 3.197 x 10^{+3} mm varying as it moves towards the fence and fence bracers on both sides within the range of 9.394 x 10^{+2} mm to 2.238 x 10^{+3} mm, leaving an even distribution on other sides of the base as low as and below 1.000 x 10^{-30} mm.

These results indicate that the MJ exhibited stress concentrations at vertical supports and fence junctions, where the workpiece pressure is highest. Maximum directional deformations occurred at the point of saw contact, confirming the structural demand in that area.

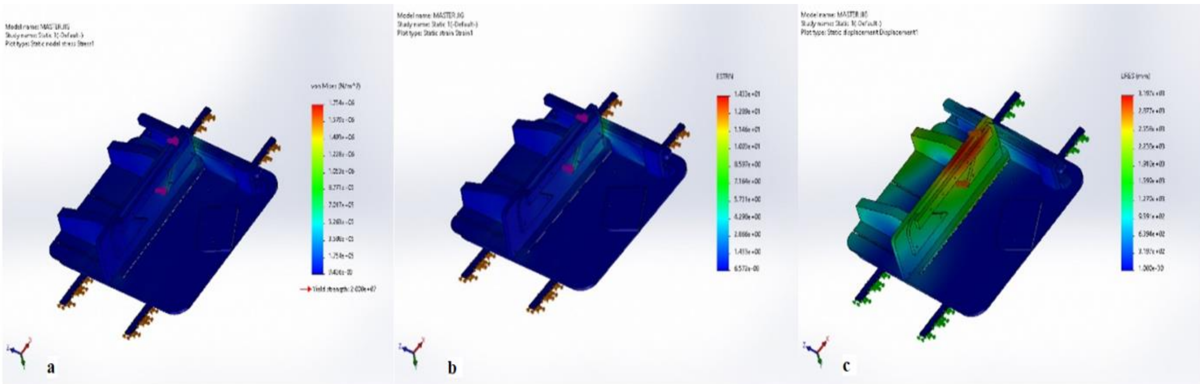

Figure 3. Distribution of von Mises stress (a), Elastic strain (b) and Displacement (c) with applied external load at 600 N

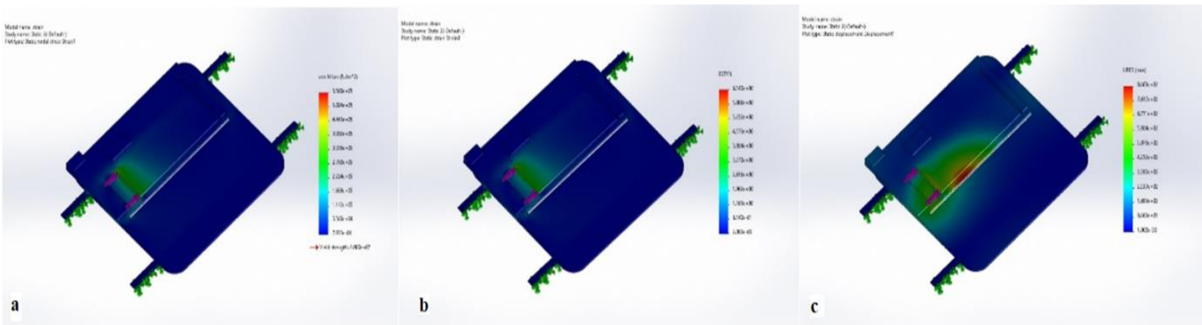

Figure 4. Distribution of von Mises stress (a), elestic strain (b) and displacement (c) with applied external load at 520 N

3.3 Factor of safety

Fig. 5a and b. shows the factor of safety value on the simulated FE model when external loads of 520N and 600N are applied. The high factor of safety (11 and 31) across both load cases confirms the jig's structural resilience and suitability for high-force cutting applications, which means that the master jig, as designed, can withstand loads that are 11 and 31 times higher than its designed load.

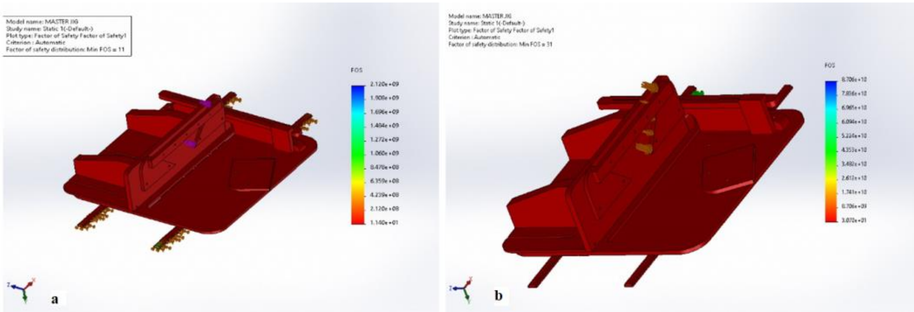

Figure 5. Factor of Safety at 520N (a) and 600N (b)

3.4 Deformation behaviour

To observe the deformation behavior (failure mode) of the FE modelled master jig at 520N and 600N applied load, the stress, strain and displacement diagram were scaled to 0.135238 and 0.036047, respectively which allows visualisation of potential failure regions. The displays shown in Figs. 6a, b, c and 7a, b, c respectively are results of localised deformation in high-stress zones, validating the design's robustness for typical woodworking forces. However, it should be noted that the true scale (Figs. 3 and 4) represents the possible deformation that can occur on the jig.

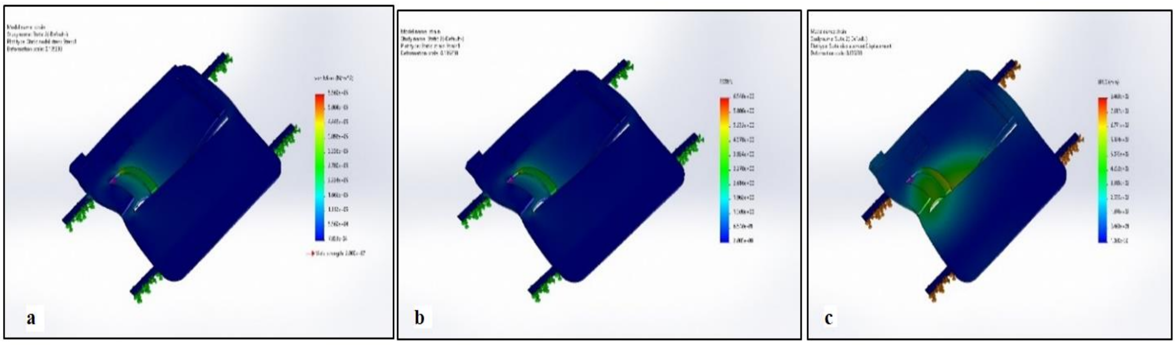

Figure 6. Deformation behavior of FE model (a) stress, (b) Strain, and (c) displacement when scaled to 0.135238 for 520N

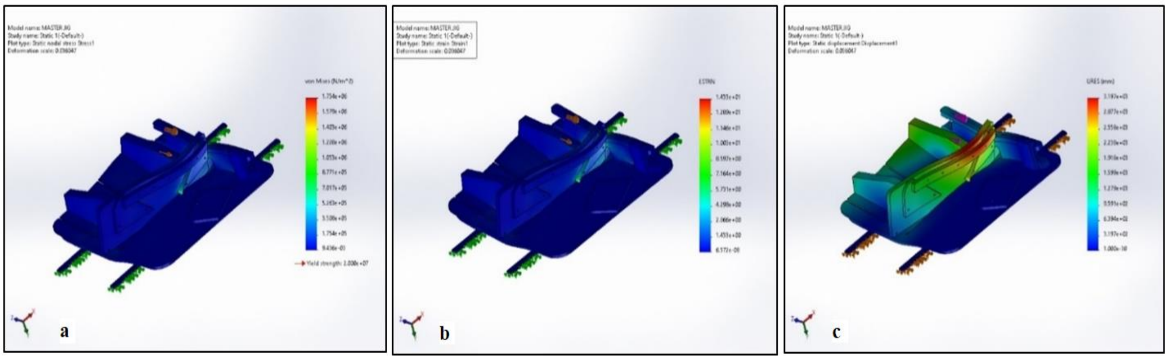

Figure 7. Deformation behavior of FE model (a) stress, (b) Strain, and (c) displacement when scaled to 0.036047 for 600N

3.5 Nodal edge plots

Fig. 8 (a-c) presents the nodal edge graph (plots) of static stress, strain and displacement along a parametric distance for the vertical work support face, respectively. The von Mises stress values decreased from 4.00 MPa to 1.00 MPa, suggesting a reduction in the stress along the parametric distance (Fig. 8a). The strain contour starts at minimum (0.00), indicating no deformation at the beginning of the parametric distance and jumps significantly to 5.00 and then to 10.00, suggesting a rapid increase in the strain over a short distance. It then decreases gradually, suggesting that the material experienced less deformation as the parametric distance increased beyond the critical point (Fig. 8b). The displacement contour starts at 1,500.00 mm and increases steadily as the distance increases, indicating a movement away from the point of maximum displacement. Table 3 presents the sum, average, maximum, minimum and root square means of the nodal edge plots for the vertical work support face.

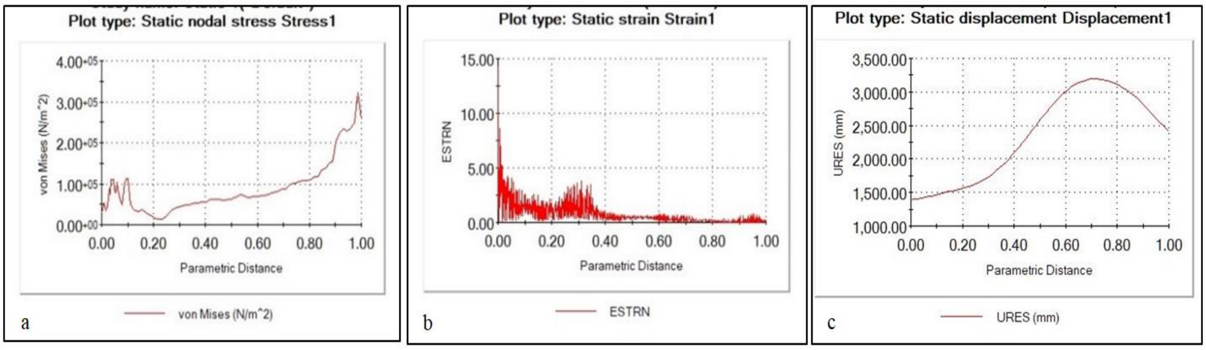

Figure 8. Static stress (a), strain (b) and Displacement (c) for the Vertical Work Support face

Fig. 9 (a-c) presents the nodal edge graph (plots) of static stress, strain and displacement along a parametric distance for the left and right vertical mitre, respectively. The von Mises stress starts at nearly 1.5 10^5 MPa with slight fluctuation around the middle area, then increasing significantly towards the end of the parametric distance. This suggests a possible stress concentration at the left and right vertical mitre (Fig. 11a). The static strain (ESTRN) plot (Fig. 9b) starts at nearly 2.00 with a slight increase and fluctuations in the middle area, and a significant spike is observed towards the tail of the parametric distance near 8.0. This sharp increase towards the end may indicate a region of high deformation, possibly near the concentration point of the L/R vertical mitre. For the displacement (Fig. 9c), an initial decrease near the minimum was observed at the parameter distance of 0.1. Afterwards, a near-linear trend is observed as the displacement gradually increases until its peak at approximately 3000 mm and a parametric distance of 1.0. The sum, average, maximum, minimum and root square means of the nodal edge plots for the left and right vertical mitre are presented in Table 3.

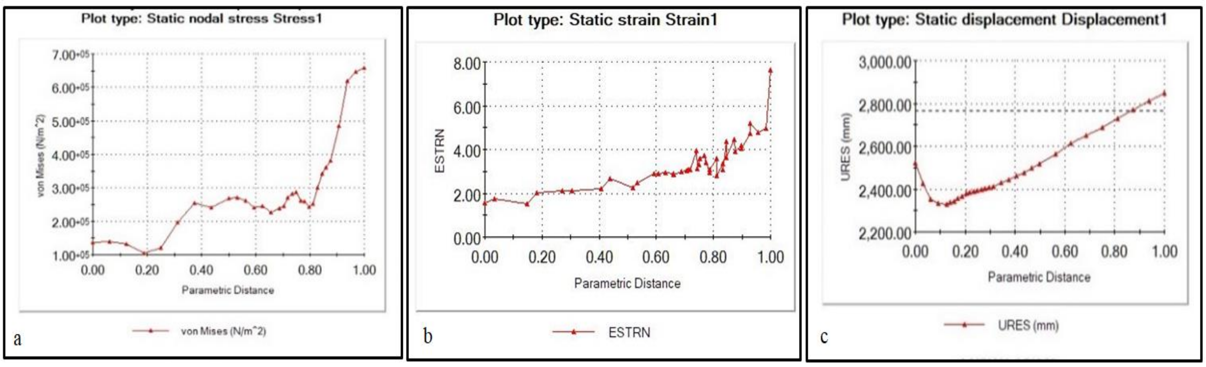

Figure 9. Static stress, strain and Displacement for the Left and Right Vertical mitre

Fig. 10 (a-c) presents the nodal edge graph (plots) of static stress, strain and displacement along a parametric distance for the adjustable stop bar, respectively. The static Nodal stress (von Mises stress) distribution contour starts very low (Fig. 10a), beginning from a 0.00-0.05 parametric distance and then moves sharply to a peak of about 9.00 Mpa in the meddle indicating a critical stress concentration and quickly drops down before getting to the end of the parametric distance of the adjustable bar. The static strain (ESTRN) plot has similar distributions to the von Mises stress (Fig. 10b). However, the static displacement (URES) distribution moderates its initial displacement from approximately 700 mm, undulating to the maximum displacement at a peak of above 1000 mm at the mid-region, and then decreasing gradually until the contour hits the flow at nearly 1.0 parametric distance. The sum, average, maximum, minimum and root square means of adjustable stop bar are presented in Table 3.

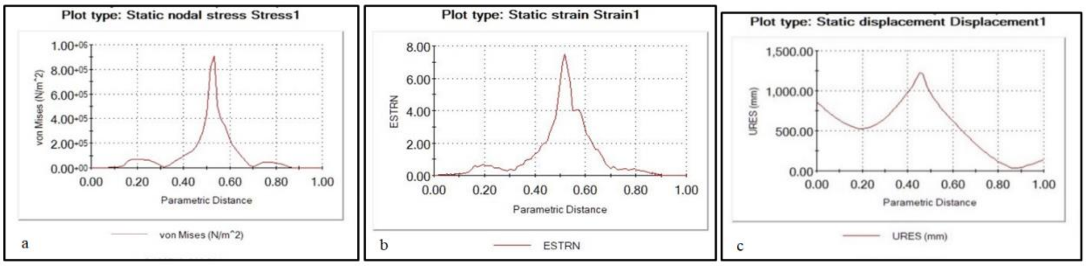

Figure 10. Static stress, strain and Displacement for the Adjustable Stop Bar

Table 3. Results based-on static nodal edge plots for simulation of different components

Object Name	von Mises Stress (MPa)	Elastic Strain	Resultant Displacement (mm)
Vertical Work Support face			
Sum	7.522 x 10^{6}	1.533 x 10^{3}	1.785 x 10^{5}
Average	8.646 x 10^{4}	8.706 x 10^{-1}	2.318 x 10^{3}
Maximum	3.221 x 10^{5}	1.433 x 10^{4}	3.197 x 10^{3}
Minimum	1.346 x 10^{4}	8.145 x 10^{-3}	1.385 x 10^{3}
RSM	1.0486 x 10^{-5}	1.370 x 100	2.403 x 10^{3}
Left and Right Vertical mitre			
Sum	8.975 x 10^{6}	1.393 x 10^{2}	7.703 x 10^{4}
Average	2.895 x 10^{5}	3.316 x 10	2.485 x 10^{3}
Maximum	6.576 x 10^{5}	7.632 x 10	2.848 x 10^{3}
Minimum	1.036 x 10^{5}	1.497 x 10	2.330 x 10^{3}
RSM	3.209 x 10^{-5}	3.499 x 10	2.489 x 10^{3}
Adjustable Stop Bar			
Sum	6.571 x 10^{6}	7.487 x 10^{1}	4.145 x 10^{4}
Average	8.113 x 10^{4}	6.568 x 10^{-1}	5.117 x 10^{3}
Maximum	9.089 x 10^{5}	7.792 x 10	1.223 x 10^{3}
Minimum	9.762 x 10	1.290 x 10^{4}	3.098 x 10^{1}
RSM	1.805 x 10^{-5}	1.508 x 10	6.109 x 10^{2}

4 Conclusions

A finite element-based approach was used to investigate the performance and deformation behaviour of the master jig on the circular saw machine as presented in this study. The following conclusions are drawn:

- The study confirms the suitability of FEM in evaluating the structural performance of a master jig for circular saw operations.
- The isotropic material assumptions provided an acceptable first-order prediction.
- The jig's performance under 520 N and 600 N loads suggest its effective use in real woodworking operations.

Future works should focus on incorporating anisotropic multi-layered MDF modelling for higher fidelity and developing additional jig types for varied cutting tasks using this modelling framework.

Author Contributions

Asibong Asibong Icha: Conceptualization, Data curation, Formal Analysis, Funding acquisition, Investigation, Methodology, Project administration, Resources, Supervision, Validation, Visualization, Writing – original draft, Writing – review & editing, **Simon Ogbeche Odey**: Funding acquisition, Project administration, Resources, Supervision, Validation, Visualization, Writing – review & editing.

Funding statement

This project was funded and supported by The Nigerian Tertiary Education Trust Fund, Institute - Based Research, with project number: TETF/DR&D/CE/UNI/CALABAR/IBR/2024/batch 8

Conflict of interest statement

The authors declare no conflict of interest.

References

Autengruber, M., Lukacevic, M., Wenighofer G., Raimund Mauritz, R., and Füssl, J., (2021). Finite-element-based concept to predict stiffness, strength, and failure of wood composite I-joist beams under various loads and climatic conditions, *Engineering Structures*, 245 112908, DOI: 10.1016/j.engstruct.2021.112908

Blomqvist, L., Ormarsson, S. and Ziethén, R., (2023). Stress distribution in veneers under lamination and simultaneously bending: an experimental and numerical investigation, *Wood Material Science & Engineering*, 18:3, 995-1002, DOI:10.1080/17480272.2022.2099762

Brischke, C., Alfredsen, G., Humar, M., Conti, E., Cookson, L., Emmerich, L., and Suttie, E., (2021). Modelling the material resistance of wood—part 3: relative resistance in above-and in-ground situations—results of a global survey. *Forests*, 12(5), 590, DOI: 10.3390/f12070959

DeCristoforo, R.J., (1988). *The Complete Book of Stationary Power Tool Techniques*. Sterling Publishing Co., Inc. Two Park Avenue, New York, N. Y. 388p

Falk, R. H., and Itani, R. Y., (1989). Finite element modeling of wood diaphragms, *Journal of Structural Engineering*, 115(3), 543-559, https://www.fpl.fs.usda.gov/documnts

Falko, F. Ehrenstein, J. Höltgen, C. Blondrath, A. Schäper, L. Göppert, A. and Schmitt, R., (2023). Jigs and fixtures in production: a systematic literature review. *Journal of Manufacturing Systems*, 72, 373–405, DOI: 10.1016/j.jmsy.2023.10.006

Frontini F., (2023) A novel approach for modelling a historic timber roof, International Wood Products Journal, 14:1, 21-33, DOI: 10.1080/20426445.2023.2171895

Fleming, S., (2020). Woodworking and Whittling for Kids, Teens and Parents: A Beginner's Guide with 51 DIY Projects for Digital Detox and Family Bonding. Stephen Fleming.

Hernández, R.E., Passarini, L. and Koubaa, A., (2014). Effects of temperature and moisture content on selected wood mechanical properties involved in the chipping process, *Wood Science and Technology*, 48, 1281-1301.

Hong, J. P., and Barrett, D., (2010). Three-dimensional finite-element modelling of nailed connections in wood, *Journal of Structural Engineering*, 136(6), 715-722. DOI: 10.1061/ASCEST.1943-541X.0000160

Huber, J. A., Broman, O., Ekevad, M., Oja, J., and Hansson, L., (2022). A method for generating finite element models of wood boards from X-ray computed tomography scans, *Computers & structures*, 260, 106702, DOI: 10.1016/j.compstruc.2021.106702

Hu, W., Yan Liu Y., and Konukcu, A. C., (2022). Study on withdrawal load resistance of screw in wood-based materials: experimental and numerical, *Wood Material Science & Engineering*, DOI: 10.1080/17480272.2022.2084699

Icha, A. A., and Odey, S. O., (2024). Development of a master jig for circular saw machine, *Nigerian Journal of Engineering Research Unicross* (NJERU) ISSN No. 2971-785X 1(2), 87-95. https://njerunicross.com.ng/assets/images/articles/1727797215_article.pdf

Icha, A. A., and Odey, S. O., (2024). Modelling and simulation of a tenoning jig to predict performance and failure mode on circular saw machine, *International Wood Products Journal*, 15(1), 44–54. DOI: 10.1177/20426445241226534

Icha A, Odey S, and Ekpe H., (2024). A finite element approach to ınvestigate the performance and reliability of an extension stand in table saw machines, *Wood Industry and Engineering*, 6(2), 1-13, https://dergipark.org.tr/en/pub/wie/issue/89190/1503930

Kumar, S. R., Campilho, R. D. S. G., and Silva, F. J. G., (2019). Rethinking modular jigs' design regarding the optimization of machining times, *Procedia Manufacturing*, 38, 876–883. DOI: 10.1016/j.promfg.2020.01.169

Massaro, F. M., and Malo, K. A., (2020). Stress-laminated timber decks in bridges: Friction between lamellas, butt joints and pre-stressing system, *Engineering Structures*, 213, 110592, ISSN 0141-0296, DOI: 10.1016/j.engstruct.2020.110592

Odey, S. O., and Icha, A. A., (2022). Finite element modelling and evaluation of a sliding table jig for mitering operations in circular saw machine, *Journal of Contemporary Research* (JOCRES) 1(2), 173 -181. ISSN: 2814-2241

Okpala, C. C., and Okechukwu, E., (2015). The design and need for jigs and fixtures in manufacturing, *Science Research*, 3(4), 213-219.

Qiu, L. P., Zhu, E. C., and Van de Kuilen, J. W. G., (2014). Modelling crack propagation in wood by extended finite element method, *European Journal of Wood and Wood Products*, 72(2), 273-283, DOI: 10.1007/s00107-013-0773-5

Radhwan, H., Effendi, M. S. M., Rosli, F.R., Shayfull, Z. and Nadia, K. N., (2019) Design and analysis of jigs and fixtures for manufacturing process, *IOP Conference Series Materials Science and Engineering*, 551(1), 012028–012028, DOI:10.1088/1757-899x/551/1/012028

Salin, J. G., (2008). Modelling water absorption in wood, Wood Material Science and Engineering, 3(3-4), 102-108. DOI: 10.1080/17480270902781576

Seward, D., (2014). Connections. In: Understanding Structures, Palgrave, London. 231 – 251, DOI: 10.1007/978-1-349-14809-7_10

SOLIDWORKS., (2021). SolidWorks 2021 [Computer software]. Dassault Systèmes.

Tankut, N., Tankut, A. N., and Zor, M., (2014). Finite element analysis of wood materials, Drvna industrija, 65(2), 159-171. DOI:10.5552/drind.2014.1254

Vasic, S., Smith, I., and Landis, E., (2005). Finite element techniques and models for wood fracture mechanics, *Wood science and technology*, 39, 3-17. DOI: 10.1007/s00226-004-0255-3

Yıldırım, M. N, Karaman, A., and Akınay, A., (2016). Finite element method application of wooden furniture, International conference on research in education science, Bodrum/Muğla/Türkiye, 19 - 22 Mayıs 2016, ss.1258-1270.

Zhong, W., Zhang, Z., Chen, X., Wei, Q., Chen, G., and Huang, X., (2021). Multi-scale finite element simulation on large deformation behaviour of wood under axial and transverse compression conditions, *Acta Mechanica Sinica*, 37, 1136-1151, DOI: 10.1007/s10409-021-01112-z